Cao et al. *Zool. Res.* 2023, 44(3): 620−635
https://doi.org/10.24272/j.issn.2095-8137.2022.340

ZR | Zoological Research

Article Open Access

Extracellular vesicles from iPSC-MSCs alleviate chemotherapy-induced mouse ovarian damage via the ILK-PI3K/AKT pathway

Rui-Can Cao[1,2,3,4,7], Yue Lv[2,5], Gang Lu[2,3,7], Hong-Bin Liu[1,3,4], Wuming Wang[2,3,7], Chunlai Tan[2,3], Xian-Wei Su[3,7], Zhiqiang Xiong[6], Jin-Long Ma[1,3,4,*], Wai-Yee Chan[2,3,7,*]

[1] *Center for Reproductive Medicine*, *Shandong University*, *Jinan*, *Shandong* 250012, *China*
[2] *Hong Kong Branch of CAS Center for Excellence in Animal Evolution and Genetics*, *The Chinese University of Hong Kong*, *Hong Kong SAR*, *China*
[3] *CUHK-SDU Joint Laboratory on Reproductive Genetics*, *School of Biomedical Sciences*, *Faculty of Medicine*, *The Chinese University of Hong Kong*, *Hong Kong SAR*, *China*
[4] *Key Laboratory of Reproductive Endocrinology of Ministry of Education*, *Shandong University*, *Jinan*, *Shandong* 250012, *China*
[5] *Shandong Key Laboratory of Reproductive Medicine*, *Shandong Provincial Hospital Affiliated to Shandong First Medical University*, *Jinan*, *Shandong* 250012, *China*
[6] *SDIVF R&D Centre, 12W, HKSTP, Hong Kong SAR, China*
[7] *Kunming Institute of Zoology - The Chinese University of Hong Kong (KIZ-CUHK) Joint Laboratory of Bioresources and Molecular Research of Common Diseases*, *Hong Kong SAR*, *China*

ABSTRACT

Chemotherapy can significantly reduce follicle counts in ovarian tissues and damage ovarian stroma, causing endocrine disorder, reproductive dysfunction, and primary ovarian insufficiency (POI). Recent studies have suggested that extracellular vesicles (EVs) secreted from mesenchymal stem cells (MSCs) exert therapeutic effects in various degenerative diseases. In this study, transplantation of EVs from human induced pluripotent stem cell-derived MSCs (iPSC-MSC-EVs) resulted in significant restoration of ovarian follicle numbers, improved granulosa cell proliferation, and inhibition of apoptosis in chemotherapy-damaged granulosa cells, cultured ovaries, and *in vivo* ovaries in mice. Mechanistically, treatment with iPSC-MSC-EVs resulted in up-regulation of the integrin-linked kinase (ILK) -PI3K/AKT pathway, which is suppressed during chemotherapy, most likely through the transfer of regulatory microRNAs (miRNAs) targeting ILK pathway genes. This work provides a framework for the development of advanced therapeutics to ameliorate ovarian damage and POI in female chemotherapy patients.

Keywords: Extracellular vesicles; Premature ovarian insufficiency; Human induced pluripotent stem cell-derived mesenchymal stem cells; ILK-PI3K/AKT pathway

INTRODUCTION

Clinical application of chemotherapy has become increasingly common, concurrent with increasing rates of cancer incidence. Cyclophosphamide (CTX) is a chemotherapeutic agent that induces DNA damage by releasing cytochrome from the mitochondria, which activates the apoptotic pathway, and consequently eliminates cells with abnormally high proliferation rates (Helleday et al., 2008). Therefore, CTX can be effective for treating various malignancies and can significantly improve survival rates of cancer patients. However, CTX can also cause serious damage to the female reproductive system. Notably, CTX can induce apoptosis in ovarian granulosa cells, cause damage to ovarian stroma, and significantly reduce ovarian tissue follicles, leading to endocrine disorders, reproductive dysfunction, and primary ovarian insufficiency (POI) (Desmeules & Devine, 2006; Meirow et al., 2010; Sonigo et al., 2019). More severe cases can cause premature ovarian failure, defined as the cessation of ovarian function prior to age 40 (Coulam et al., 1986;

Received: 26 October 2022; Accepted: 01 March 2023; Online: 02 March 2023

Foundation items: This work was supported by the CUHK VC Discretionary Fund provided to the Hong Kong Branch of Chinese Academy of Science Center for Excellence in Animal Evolution and Genetics (Acc 8601011), the National Key R&D Program (2021YFC2700500), A-Smart Group to Shandong University and SDIVF R&D Centre Hong Kong, and Research Grants Council General Research Fund (Hong Kong Special Administrative Region Government) (14103418)

*Corresponding authors, E-mail: majinlong_sdu@163.com; chanwy@cuhk.edu.hk

Jankowska, 2017; Jiao et al., 2018). POI is characterized by amenorrhea, low estrogen, high gonadotropins, infertility, and reduced follicle counts, with chemotherapy reported to be one of the most common causes of POI in female cancer patients (Jankowska, 2017; Qin et al., 2015). To date, no specific drug exists for effective intervention in POI, and once it occurs, it is difficult to reverse. Thus, protection against chemotherapy-induced reproductive toxicity represents a major concern for young and fertile women with cancer.

Recent discoveries regarding the function of stem cell-secreted extracellular vesicles (EVs, small 40–100 nm particles) suggest the possibility of major advances in regenerative medicine (Basu & Ludlow, 2016; Jing et al., 2018; Nagelkerke et al., 2021). The regenerative benefits of stem cell transplantation are partially due to the paracrine effects of EV release (Takahashi et al., 2021; Zhang et al., 2017, 2019). Notably, EVs do not contain MHC I or MHC II proteins, do not increase the risk of immunogenicity, and are not tumorigenic, thus overcoming several disadvantages of cell transplantation therapies (Qi et al., 2016; Zhang et al., 2015). Several studies have found that EVs derived from mesenchymal stem cells (MSCs) can promote tissue repair (Harrell et al., 2019; Tang et al., 2021). Furthermore, EVs secreted by bone marrow stem cells can rescue fertility in mice with CTX-induced POI (Yang et al., 2020). In addition, MSC-derived EVs, such as those from adipose MSCs (Huang et al., 2018), human amniotic MSCs (Ding et al., 2020a), or human umbilical cord MSCs (Yang et al., 2019), can restore partial ovarian function in CTX-induced mouse models of POI. These findings suggest that MSC-EVs may have the potential to rescue ovarian function in chemotherapy-induced POI, although these MSCs display limited proliferation *in vitro* and their acquisition is highly invasive. Therefore, alternative sources of MSC-EVs are urgently needed to develop effective and widely available clinical applications. Germane to this issue, human induced pluripotent stem cell-derived MSCs (iPSC-MSCs) can be induced to differentiate from a wide variety of cells, are easily obtained, and can be expanded indefinitely. Previous studies have shown that iPSC-MSCs secrete EVs that promote wound repair (Zhang et al., 2015), angiogenesis (Hu et al., 2015), and bone regeneration (Qi et al., 2016). To date, however, no reports have examined the use of iPSC-MSC-EVs in POI.

In the present study, we investigated the therapeutic effects of iPSC-MSC-EVs in a CTX-induced mouse model of ovarian injury. Results showed that iPSC-MSC-EVs significantly attenuated ovarian injury. A significant increase in follicle number was observed in POI mice after iPSC-MSC-EV treatment. The same phenotype was found in cultured CTX-damaged ovaries *in vitro.* Exposure to iPSC-MSC-EVs enhanced proliferation and inhibited apoptosis of granulosa cells. Specifically, iPSC-MSC-EV treatment up-regulated ILK transcription and protein levels *in vivo* and *in vitro*. Overall, iPSC-MSC-EVs inhibited granulosa cell apoptosis, accelerated cell cycle, and promoted cell proliferation by activating the ILK pathway. We found that iPSC-MSC-EVs conferred restorative effects on the ovaries of mice with POI, supporting the further development of iPSC-MSC-EVs as an advanced therapeutic for treating chemotherapy-induced ovarian injury or POI in female cancer patients.

MATERIALS AND METHODS

Induction of iPSCs

Human dermal fibroblasts (HDFs) (ATCC #PCS-201-010, USA) were cultured with Dulbecco's Modified Eagle Medium (DMEM) (Gibco, USA) supplemented with 10% fetal bovine serum (FBS) (Gibco, USA) and 1% penicillin/streptomycin (Gibco, USA) for 48 h at 37 °C. Plasmids UL (Addgene #27080, USA), OP (Addgene #27077, USA), and SK (Addgene #27078, USA) were mixed and electroporated into HDFs using a NEPA21 electroporator (Nepagene, Japan) based on previous protocols (Okita et al., 2011, 2013). The transfected cells were then seeded on Matrigel-coated plates (Corning #354277, USA) and cultured with mTeSR (STEMCELL #85850, Canada) at 37 °C, with the medium changed every two days. Colonies were evaluated 24–29 days after plating and those similar to human embryonic stem cells (ESCs) were selected for further culture. in a 15 mL Amicon Ultra-15 centrifugal filter unit (Millipore #UFC910024, USA). The ultra-filtered suspension was washed twice with 15 mL of phosphate-buffered saline (PBS) and ultra-filtered to 200 μL at 4 000 ×*g* for 15 min. All procedures were performed at 4 ºC. The iPSC-MSC-EVs were stored at −80 °C (Lobb et al., 2015).

Alkaline phosphatase (AP) staining

iPSCs are in an undifferentiated state characterized by high levels of AP expression, indicating the potential for self-renewal. Here, AP activity in iPSCs was detected using an AP Staining Kit II (STEMGENT #00-0055, USA) according to the product manual. Images were recorded using a Nikon fluorescence microscope (Japan).

Derivation and characterization of iPSC-MSCs

The iPSCs were induced to differentiate into MSCs using a Mesenchymal Progenitor Cell Kit (STEMCELL, USA). The medium was changed to low-glucose DMEM (Gibco, USA) supplemented with 10% FBS (Gibco, USA), 1% penicillin/streptomycin (Gibco, USA), and 2 mmol/L L-glutamine (Gibco, USA) when the cells exhibited a fibroblast-like morphology after day 21.

Flow cytometry analysis

The iPSC-derived MSCs were identified at the second passage and sorted using a Beckman Coulter flow cytometry system (FC500) (USA). After labeling with antibodies CD73-APC, CD90-FITC, CD105-PerCP, and CD45/CD34/CD11b/CD19/HLA-DR-PE (BD Biosciences #562245, USA), cells expressing MSC-specific markers CD73, CD90, and CD105 and no negative markers (CD45/CD34/CD11b/CD19/HLA-DR) were collected and considered as successfully differentiated MSCs (Dominici et al., 2006).

Isolation and characterization of iPSC-MSC-EVs

When the iPSC-MSCs (passage 3–7) reached 80%–90% confluence, the culture medium was replaced by complete medium without FBS and incubated for another 48 h before collection. To remove dead cells and cellular debris, the conditioned medium (CM) of the iPSC-MSCs was centrifuged at 300 ×*g* for 10 min, then at 2 000 ×*g* for 10 min. The CM was then filtered through a 0.22 μm filter sterilizer and ultra-filtered to approximately 200 μL at 4 000 ×*g* for 20 min–1 h in a 15 mL Amicon Ultra-15 centrifugal filter unit (Millipore #UFC910024, USA). The ultra-filtered suspension was washed twice with 15 mL of phosphate-buffered saline (PBS) and ultra-filtered to 200 μL at 4 000 ×*g* for 15 min. All procedures were performed at 4 ºC. The iPSC-MSC-EVs were stored at −80 °C (Lobb et al., 2015).

Transmission electron microscopy (TEM) was used to

detect the morphology and size of iPSC-MSC-EVs. A bicinchoninic acid (BCA) protein quantification kit (Beyotime #P0010S, China) was used to evaluate protein concentration. The presence of exosomal characteristic surface marker proteins CD9 (Santa Cruz, USA), CD63 (Abcam, UK), CD81(Santa Cruz, USA), and HSP 70 (Abcam, UK) and negative marker CALNEXIN (Santa Cruz, USA) was analyzed by western blotting. The size distribution of iPSC-MSC-EVs was determined using a flow nanoanalyzer (NanoFCM N30E, China). RNA distribution of iPSC-MSC-EVs was assessed using the Agilent 2100 Bioanalyzer system (Agilent, Amstelveen, Netherlands) (Supplementary Figure S1).

Experimental animals

Wild-type C57BL/6J female mice (postnatal day 2 (PD2)–PD3, PD20–23, PD28) were provided by the Laboratory Animal Experimental Service Center at the Chinese University of Hong Kong (CUHK) and Laboratory Animal Center of Shandong University (SDU). All experimental procedures were approved by the Animal Experimentation Ethics Committee of CUHK (Ref No. 20-048-MIS) and the Ethics Review Board of the Center for Reproductive Medicine of SDU.

Animal groups and treatments

We obtained 28-day-old C57/6j female mice (*n*=36) from the Laboratory Animal Center of SDU and randomly assigned them to three equal groups. Mice assigned to the control group (*n*=12) received no treatment. Mice assigned to the chemotherapy-treated (CTX) group (*n*=12) and chemotherapy plus iPSC-MSC-EV co-treated (CTX-EV) group (*n*=12) received intraperitoneal injections of CTX (120 mg/kg) (Sigma-Aldrich, USA) once a week for two weeks to induce ovarian damage (Huang et al., 2018). During chemotherapy, mice in the CTX-EV group received 200 μg of EVs (approximate amount produced by 5×10^6 iPSC-MSCs) in 200 μL of PBS via tail vein injection once every three days six times, while mice in the CTX group received an equal amount of PBS in the tail vein (see Supplementary Figure S2A for specific experimental workflow).

***In vitro* ovary culture**

Ovaries from PD2–PD3 mice were harvested in Leibovitz's L-15 medium (Gibco, USA) containing 5% FBS (Gibco, USA), then cultured on the surface of 0.4 μm pore size cell culture inserts (Millipore #PICM0RG50, USA) placed in 6-well plates. The ovaries were cultured in DMEM/F12 (Gibco, USA) supplemented with 1 mg/mL BSA (Gibco, USA), 1 mg/mL AlbuMAX II (ThermoFisher Scientific, USA), 5% insulin-transferrin-selenium (ITS-G) (ThermoFisher Scientific, USA), 100 μmol/L L-ascorbic acid (ThermoFisher Scientific, USA), and 1% penicillin-streptomycin (Gibco, USA).

During ovarian culture, 4-hydroxycyclophosphamide (4HC-CTX, 10 μmol/L) (Santa Cruz, CAS 39800-16-3, USA) and iPSC-MSC-EVs (100 μg/mL) were added to the medium based on the group. The ovaries were cultured in a humidified incubator at 37 °C with 5% CO_2 for 72 h. The culture medium was changed every other day. After *in vitro* culture, the ovaries were collected for histological and immunohistochemical (IHC) analysis.

Histological analysis

Mouse ovaries were fixed in 4% paraformaldehyde (PFA) solution, dehydrated, and embedded in paraffin. Ovaries were serially sectioned at 5 μm. For adult ovaries, one of every five sections was selected for hematoxylin staining. Ovarian morphology was observed and photographed with an optical microscope (Nikon, Japan). Primordial, primary, secondary, and mature follicles were classified according to well-accepted standards (Pedersen & Peters, 1968). To calculate total follicles, the number of follicles in all stages was multiplied by a correction factor of 5. For ovaries cultured *in vitro*, one of every two sections was selected for hematoxylin staining and the number of follicles in all stages was multiplied by a correction factor of 2.

Immunohistochemistry

Ovarian paraffin sections were dewaxed with xylene and rehydrated with an alcohol gradient before IHC analysis. After heating and repair in sodium citrate solution, the samples were blocked with H_2O_2 and 10% horse serum. Sections were incubated at 4 °C overnight with primary antibodies, including anti-CLEAVED CASPASE3 (1:400, CST #9664, USA), anti-KI67 (1:500, Santa Cruz #sc-15402, USA), anti-ILK1(1:100, CST #3862, USA), and anti-MVH (1:200, Abcam #ab13840, UK). The next day, all sections were washed with PBS and incubated with secondary antibodies for 1 h at room temperature. Bound antibodies were detected using a biotin-streptavidin horseradish peroxidase(HRP) detection system (ZSGB-BIO #SP-9000, China). 3,3'-diaminobenzidine (DAB) (Abcam, UK) staining was performed for 2 min at room temperature. Cell nuclei were counterstained with Mayer's hematoxylin for 5 min.

Five fields in each section were randomly selected for examination. Immunoreactive scores (IRS) (Remmele & Stegner, 1987) were used to score the staining results. Briefly, the intensity of the staining signal was classified as "0" (negative), "1" (weak), "2" (moderate), or "3" (strong) and the extent of the stained cells was classified as "0 (<5%), "1 (5%–25%), "2" (25%–50%), "3" (50%–75%), or "4" (>75%). The final IHC staining score was obtained by multiplying the two fractions together.

Granulosa cell culture

Granulosa cells were harvested from 20–23-day-old C57BL/6J mice treated with pregnant horse serum gonadotropin (PMSG) (SANSHENG #110041282, China) for 24 h. Briefly, mouse ovaries were punctured with a 26.5-gauge needle in Leibovitz' s L15 medium (Gibco, USA) to release granulosa cells. The cells were then filtered with a 0.45 μm filter (Sigma-Aldrich, USA) and cultured at a density of 1×10^6 in DMEM\F12 (Gibco, USA) containing 10% FBS (Gibco, USA) and 1% penicillin-streptomycin (Gibco, USA) for the following experiments (Liu et al., 2017).

Cell viability assay

Granulosa cells were seeded into a 96-well plate and cultured overnight in a humidified incubator at 37 °C. Apoptosis was induced the next day with 2 mg/mL or 4 mg/mL CTX (cyclophosphamide monohydrate, Sigma-Aldrich C0768, USA). Different concentrations of EVs or cultured CM from iPSC-MSCs (passage 3–7) were simultaneously added to the granulosa cells. After 24 h of treatment, MTS (Promega #G3580, USA) was used to detect cell viability according to the manufacturer's protocols. All experiments were performed in triplicate.

Western blotting

Proteins from cells and ovarian tissues were extracted using RIPA lysis buffer (Thermo # 89900, USA) containing protease inhibitor cocktail (Bimake #B14001, USA). After centrifugation

at 14 000 ×*g* for 15 min at 4 ℃, the supernatant was collected and denatured with sodium dodecyl-sulfate polyacrylamide gel electrophoresis (SDS-PAGE) loading buffer (CWBIO #CW0027, China). The iPSC-MSC-EVs were dissolved in PBS and directly denatured with SDS-PAGE loading buffer (CWBIO #CW0027, China). Protein concentrations were determined using a BCA assay (Beyotime #P0010, China). In total, 10 μg or 20 μg of protein was loaded onto 12% polyacrylamide gels for separation by electrophoresis, then transferred to polyvinylidene fluoride (PVDF) membranes (Immobilon-P #IPVH00010, USA). The membranes were blocked in 5% non-fat dry milk in Tris-buffered saline Tween-20 (TBST) for 1 h, then incubated overnight at 4 ℃ with primary antibodies, including anti-GAPDH (1:2 000, Abcam #ab9485, UK), anti-CD9 (1:200, Santa Cruz #13118, USA), anti-CD81 (1:100, Santa Cruz #sc-166029, USA), anti-CD63 (1:1 000, Abcam #ab216130, UK), anti-HSP70 (1:1 000, Abcam #ab137680, UK), anti-CALNEXIN (1:200, Santa Cruz #sc-23954, USA), anti-β-ACTIN (1:2 000, CST #4967, USA), anti-CASPASE3 (1:1 000, CST #9662s, USA), anti-CLEAVED CASPASE3 (1:500, CST #9664, USA), anti-PCNA (1:1 000, Santa Cruz #sc-56, USA), anti-ILK1(1:1 000, CST #3862, USA), anti-p-AKT (Ser473) (1:1 000, CST #4060, USA), anti-AKT(1:1 000, CST #4691, USA), anti-PTEN (1:1 000, CST #9188, USA), anti-CCNB1 (1:500, Sangon Biotech #D160234, China), CCND1(1:200, Santa Cruz #sc-8396, USA), and anti-P27 (1:200, Santa Cruz #sc-1641, USA). The membranes were then incubated with HRP-conjugated secondary antibodies (anti-rabbit, 1: 2 000, CST #7074S, USA or anti-mouse, 1: 2 000, CST #7076S, USA) for 1 h at room temperature. Protein bands were visualized by enhanced chemiluminescence (Immobilon ECL Ultra Western HRP Substrate, Millipore, USA) and Lucent Blue X-ray film (Advansta, USA) or the Tanon 5200 analysis system (China).

The relative intensities of the protein bands were analyzed by ImageJ 1.51 (NIH, USA). β-actin level was used as an internal standard. All experiments were repeated three times, and representative images were taken.

RNA extraction and quantitative real-time polymerase chain reaction (qRT-PCR)

Total RNA was extracted from cells using TRIzol reagent (ThermoFisher Scientific, USA) according to the manufacturer's instructions, then reverse transcribed to generate cDNA (Takara #RR047A, Japan). QRT-PCR was performed using a 384-well optical plate with the QuantStudio 7 Flex Real-time PCR System (Applied Biosystems, USA) and SYBR Green Master Premix Ex Taq (Takara, Japan). The following primer sequences were used: *ILK:* forward, 5'-GAACGACCTCA ATCAGGGGG-3'; reverse, 5'-CATTAATCCGTGCTCCACGC-3'; *Bcl2*: forward, 5'-GAACTGGGGGAGGATTGTGG-3'; reverse, 5'-GCATGCTGGGGCCATATAGT-3'; *Bax*: forward, 5'-TGAAGACAGGGGCCTTTTTG-3'; reverse, 5'-AATTCGCC GGAGACACTCG-3'; *Krt18*: forward, 5'-ACCACCAAGTC TGCCGAAAT-3'; reverse, 5'-CCGAGGCTGTTCTCCAAGTT-3'; *Ccnd1*: forward, 5'-CAACTTCCTCTCCTGCTACCG-3'; reverse, 5'-GATGGAGGGGGTCCTTGTTTAG-3'; *Vegfa*: forward, 5'-GCACATAGAGAGAATGAGCTTCC-3'; reverse, 5'-CTCCGCTCTGAACAAGGCT-3'; *Ptgs2*: forward, 5'-CATC CCCTTCCTGCGAAGTT-3'; reverse, 5'-CATGGGAGTTGG GCAGTCAT-3'; *Cdkn2a*: forward, 5'-CGCTTCTCACC TCGCTTGT-3'; reverse, 5'-AGTGACCAAGAACCTGCGAC-3'; *Pten*: forward, 5'-TGGATTCGACTTAGACTTGACCT-3'; reverse, 5'-GCGGTGTCATAATGTCTCTCAG-3'; *Gapdh*-: forward, 5'-GAGAGTGTTTCCTCGTCCCG-3'; and reverse, 5'-ACTGTGCCGTTGAATTTGCC-3'. Mouse-*Gapdh* was used for internal normalization. The $2^{-\Delta\Delta Ct}$ method was employed to determine relative mRNA expression levels (Livak & Schmittgen, 2001).

RNA sequencing (RNA-seq) and bioinformatics analysis

Total RNA was isolated from mouse granulosa cells in the control, CTX (2 mg/mL)-treated, and CTX (2 mg/mL) plus iPSC-MSC-EVs (20 μg/mL)-co-treated groups using TRIzol reagent according to the instructions. RNA was converted into a template molecule library for sequencing using the BGISEQ-500 platform (BGI, China). Kyoto Encyclopedia of Genes and Genomes (KEGG) enrichment analysis was performed using the Dr. Tom Data Analysis System (https://biosys.bgi.com). Advanced volcano plots were constructed using OmicStudio tools (https://www.omicstudio.cn/tool). Ingenuine Pathway Analysis (IPA) of regulated genes (Krämer et al., 2014) was performed to identify the most significantly associated pathways with *P*-values determined based on right-tailed Fisher's exact test, while overall activation or repression status of enriched pathways was determined by *Z*-score prediction. Statistical analysis and heatmaps were generated using Qlucore Omics Explorer.

MicroRNA (miRNA)-seq and bioinformatics analysis

RNA of iPSC-MSC-derived EVs was isolated using a miRCURY RNA Isolation Kit (Exiqon #300112, Denmark) and sequenced using the DNBSEQ platform (BGI, Shenzhen, China). Bioinformatics databases miRWalk (http://mirwalk.umm.uni-heidelberg.de/) and miRTarBase (https://mirtarbase.cuhk.edu.cn/) were used to predict the top 50 expressed miRNAs targeting *PTEN*. Correlation network analysis of overlapping miRNAs and *PTEN* was performed using OmicStudio tools (https://www.omicstudio.cn/tool). Gene Ontology (GO) enrichment analysis of the top 50 expressed miRNA-targeted genes was performed using the Dr. Tom Data Analysis System (https://biosys.bgi.com). DIANA-miRPath v3.0 (https://dianalab.e-ce.uth.gr/html/mirpathv3/) was used to identify significant KEGG pathways associated with the top 50 miRNAs in the iPSC-MSC-EVs (Vlachos et al., 2015).

RNase treatment of iPSC-MSC-EVs

The iPSC-MSC-EVs were treated with 100 μg/mL RNase A (Beyotime #ST578, China) for 1 h at 37 °C. The reaction was terminated by the addition of 400 U/mL RNase inhibitor (Beyotime #R0102-2kU, China). The iPSC-MSC-EVs were then resuspended in PBS and ultra-filtered using an Amicon Ultra-15 centrifugal filter unit (Millipore #UFC910024, USA) for washing (Ranghino et al., 2017; Sun et al., 2019).

ILK overexpression and inhibition

Mouse granulosa cells were prepared and infected at a multiplicity of infection (MOI) of 800 (Zhang et al., 2014) with vector control or ILK-overexpressing lentiviruses (GeneChem, China) for 16 h at 37 °C in the presence of 8 μg/mL polybrene. The granulosa cells were then washed and cultured in fresh medium for 48 h at 37 °C before further experiments. Both qRT-PCR and western blot analysis were performed to verify transduction efficiency. Small-molecule IN-ILK3 (MedChemExpress #HY-115677, USA) is a competitive adenosine triphosphate (ATP) inhibitor of ILK (Fang et al., 2018). IN-ILK3 was dissolved in dimethyl sulfoxide at a concentration of 50 mmol/L and stored at −80 °C before use.

The granulosa cells were divided into control, ILK-IN3 (10 μmol/L), and ILK-IN3 (10 μmol/L) plus iPSC-MSC-EV (20 μg/mL) co-treatment groups. After 48 h of treatment, the proteins were collected for additional experiments.

Statistical analysis

Data are expressed as mean±standard deviation (*SD*), with *: $P<0.05$, **: $P<0.01$, and ***: $P<0.001$ indicating statistically significant differences. Student's *t*-test and one-way analysis of variance (ANOVA) followed by Bonferroni's *post hoc* test were used where appropriate. All statistical analyses were performed using GraphPad Prism v9 (USA).

RESULTS

Generation and identification of iPSC-MSCs and iPSC-MSC-EVs

To induce the dedifferentiation of HDFs into human iPSCs, we followed previously published protocols (Okita et al., 2011, 2013). AP staining showed the proportion of plasmid-positive cells, which indicated that pluripotency was successfully induced (Figure 1A).

Morphological observations revealed characteristic changes associated with the subsequent induction of iPSCs into MSCs using a Mesenchymal Progenitor Kit (Figure 1B). Specifically, the nuclear-to-cytoplasmic volume ratio gradually decreased as most iPSCs adopted the typical MSC spindle shape by day 17. After 21 days of differentiation, MSCs expressing surface markers CD73, CD90, and CD105 without negative markers (CD45/CD34/CD11b/CD19/HLA-DR) were collected by fluorescence-activated cell sorting (FACS) (Figure 1C).

Subsequent TEM observations revealed the presence of iPSC-MSC-EVs isolated from the iPSC-MSC culture medium as round, cup-like exosomal structures with a diameter of approximately 40–150 nm (Figure 1D). Western blotting also showed that the EVs were positive for exosomal surface markers CD63, CD9, CD81, and Hsp70, but did not express exosomal negative marker CALNEXIN (Figure 1E). Based on the flow nanoanalyzer, the iPSC-MSC-EVs were mainly distributed between 50 and 100 nm, with a mean diameter of 74.14 nm (Figure 1F). Assessment of the size distribution of RNA extracted from the iPSC-MSC-EVs using the Agilent 2100 Bioanalyzer revealed enrichment of RNA fragments between 20 and 200 nt, significantly different from the RNA size distribution in cells (Supplementary Figure S1). Taken together, these results demonstrate the production and isolation of EVs in CM of iPSC-MSCs.

iPSC-MSC-EVs protected follicular development from chemotherapy-induced ovarian damage *in vivo* and *in vitro*

Recent studies have reported that iPSC-MSC-EVs can promote tissue regeneration and confer protection against tissue damage (Qi et al., 2016; Xia et al., 2020; Zhang et al., 2015). To investigate whether iPSC-MSC-EVs provide similar protection against chemotherapy-injured ovaries *in vivo*, 28-day-old C57/6j mice (n=36) were randomly divided into a CTX-treated group with induced ovarian damage, a CTX-EV-co-treated group, and an untreated control group (Figure 2A; see Supplementary Figure S2A for specific experimental workflows). No significant differences in body weight were observed among the groups on days 0, 4, 8, 11, 15, and 18 (Figure 2B).

In the control group, many normal follicles at different stages of development were observed in the ovaries. In contrast, the CTX mouse ovaries showed an abnormal morphology and a greatly reduced number of follicles, mainly consisting of mesenchymal cells in a fibrous matrix (Figure 2C). The number of primordial follicles was significantly lower in the CTX mice than in the other two groups ($P<0.001$), while primary follicles were also significantly lower than that in the controls (Figure 2D). Secondary and mature follicles showed no significant differences among the three groups.

Consistent with previous research (Huang et al., 2018), our data showed that chemotherapy severely damaged ovarian reserves (primordial follicular pool). To investigate whether iPSC-MSC-EVs exerted protective effects against apoptosis in primordial follicles after chemotherapy, we collected the ovaries from 2.5-day-old mice for *in vitro* culture, as only these follicles are present at this time. We investigated whether EV treatment affected the development of CTX-injured primordial follicles into primary follicles. Based on previous studies (Piasecka-Srader et al., 2015), we selected 4HC-CTX, an active cyclophosphamide metabolite, to treat *in vitro*-cultured ovaries. The cultured ovaries (n=36) were divided into control, 4HC-CTX (10 μmol/L), and 4HC-CTX plus iPSC-MSC-EVs (100 μg/mL) (4HC-CTX-EV) treatment groups (Figure 2A). After 72 h, hematoxylin staining revealed many morphologically normal primordial follicles in the ovarian cortex of the control group compared to the 4HC-CTX-treated ovaries, which were smaller, atrophied, and displayed abnormal cell morphology (Figure 2E).

Follicle counts showed significantly fewer primordial follicles in ovaries cultured with 4HC-CTX than in the control group ($P<0.001$). However, the number of primary follicles was significantly higher in ovaries co-treated with 4HC-CTX-EV than in the 4HC-CTX group ($P<0.001$). No significant differences in primary follicles were found among the three groups (Figure 2F). In addition, IHC staining for germ cell-specific marker MVH revealed a significant decrease in oocyte number in the 4HC-CTX group, but a significant increase in the 4HC-CTX-EV groups (Supplementary Figure S2B). These results suggest that iPSC-MSC-EVs may protect against chemotherapy-induced death of primordial follicles *in vivo* and *in vitro*.

iPSC-MSC-EVs protected ovaries from chemotherapy-induced damage by inhibiting granulosa cell apoptosis and improving proliferation

To gain further insight into the nature and extent of tissue damage in each group, we examined the expression of apoptotic marker CLEAVED CASPASE 3 in the ovaries of adult mice from each treatment group (Figure 3A). IHC staining of ovarian sections showed that CLEAVED CASPASE 3 was significantly higher in the CTX group, especially in the granulosa cells, confirming the severity of damage in these cells. Interestingly, the prevalence of apoptotic granulosa cells decreased significantly after injection with iPSC-MSC-EVs, implying that iPSC-MSC-EVs may confer some protection against chemotherapy-induced ovarian damage. Further IHC staining of these ovarian sections for proliferation marker KI67 indicated that although KI67 levels decreased after CTX exposure, treatment with iPSC-MSC-EVs at least partially restored expression. These results suggest that exposure to iPSC-MSC-EVs can, to some extent, reverse chemotherapy-induced inhibition of cell proliferation in ovaries and promote

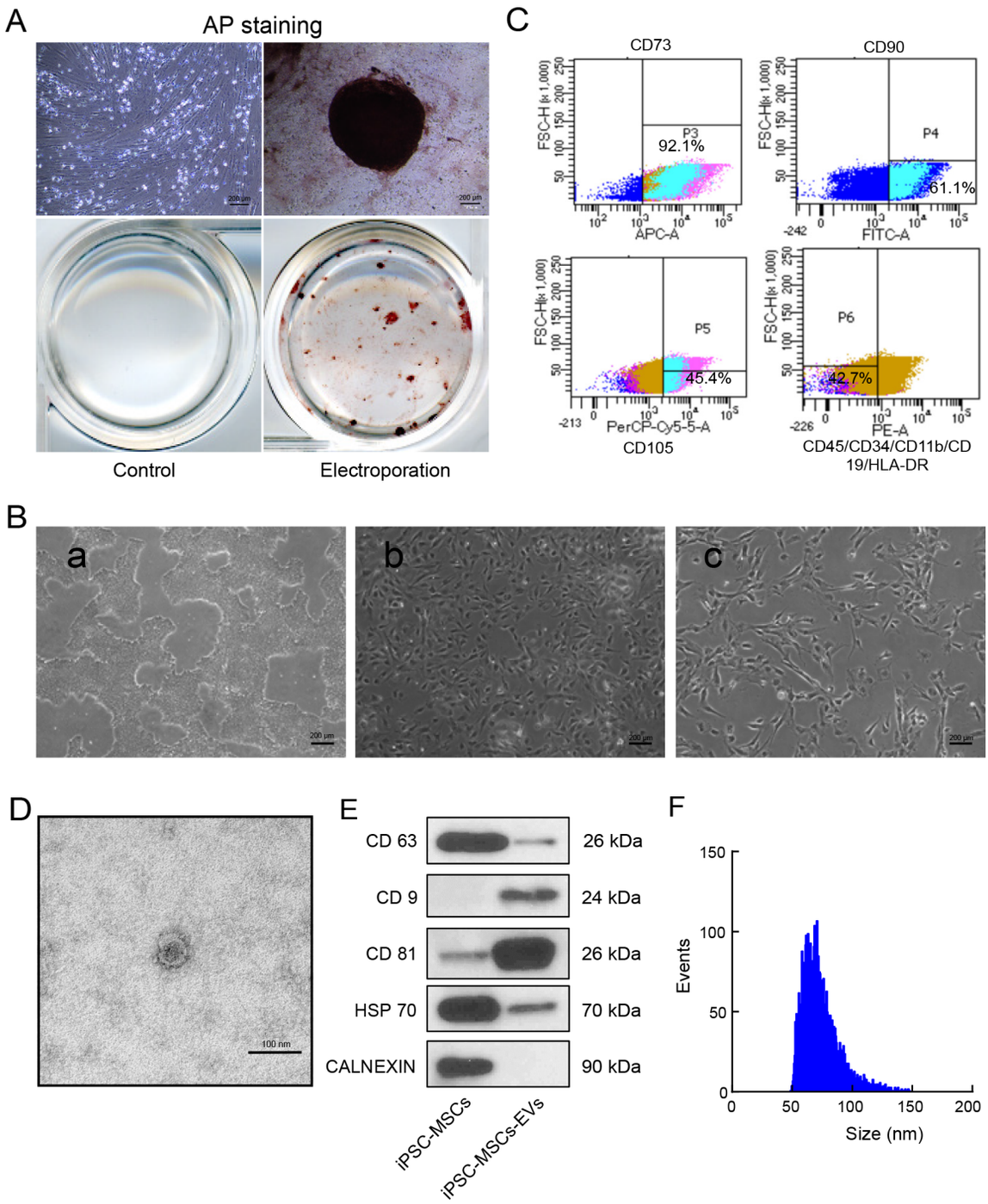

Figure 1 Characterization of human iPSC-MSCs and iPSC-MSC-EVs

A: iPSCs induced by fibroblasts were positive for AP staining, indicating successful induction of pluripotency. B: Differentiation and characterization of human iPSC-MSCs. Scale bars: 200 μm. a: Representative cell morphology of iPSCs before differentiation; b: Intermediate phase of differentiating iPSCs into MSCs; c: Typical fibroblast-like morphology of cells. C: iPSC-MSCs expressing MSC surface markers CD73, CD90, and CD105 and no negative markers (CD45/CD34/CD11b/CD19/HLA-DR) were sorted and collected by FACS. D: TEM images of iPSC-MSC-EV morphology. Scale bars: 100 nm. E: Western blot analysis of exosome-related markers CD9, CD63, CD81, and HSP70, with CALNEXIN used as a negative control. F: Particle size distribution of iPSC-MSC-EVs determined by flow nanoanalyzer.

ovarian recovery. These results were verified in the cultured ovaries (Figure 3B). Notably, CLEAVED CASPASE 3 was highly expressed in the 4HC-CTX-treated ovaries but reduced in the 4HC-CTX-EV-co-treated ovaries. Furthermore, KI67 levels were decreased in the 4HC-CTX-treated group but were increased in the combined treatment group *in vitro*.

Granulosa cells are susceptible to chemotherapy-induced damage (Huang et al., 2018; Yang et al., 2020; Zhang et al., 2019), and granulosa cell death can have detrimental effects on follicle survival. Based on our findings, we hypothesized that iPSC-MSC-EVs may be capable of rescuing chemotherapeutic drug-induced apoptosis in granulosa cells and potentially promote their proliferation. To investigate this possibility, granulosa cells were isolated from the ovaries of 20–23-day-old female mice and subjected to CTX in combination with EVs at a range of doses *in vitro* (Figure 3C).

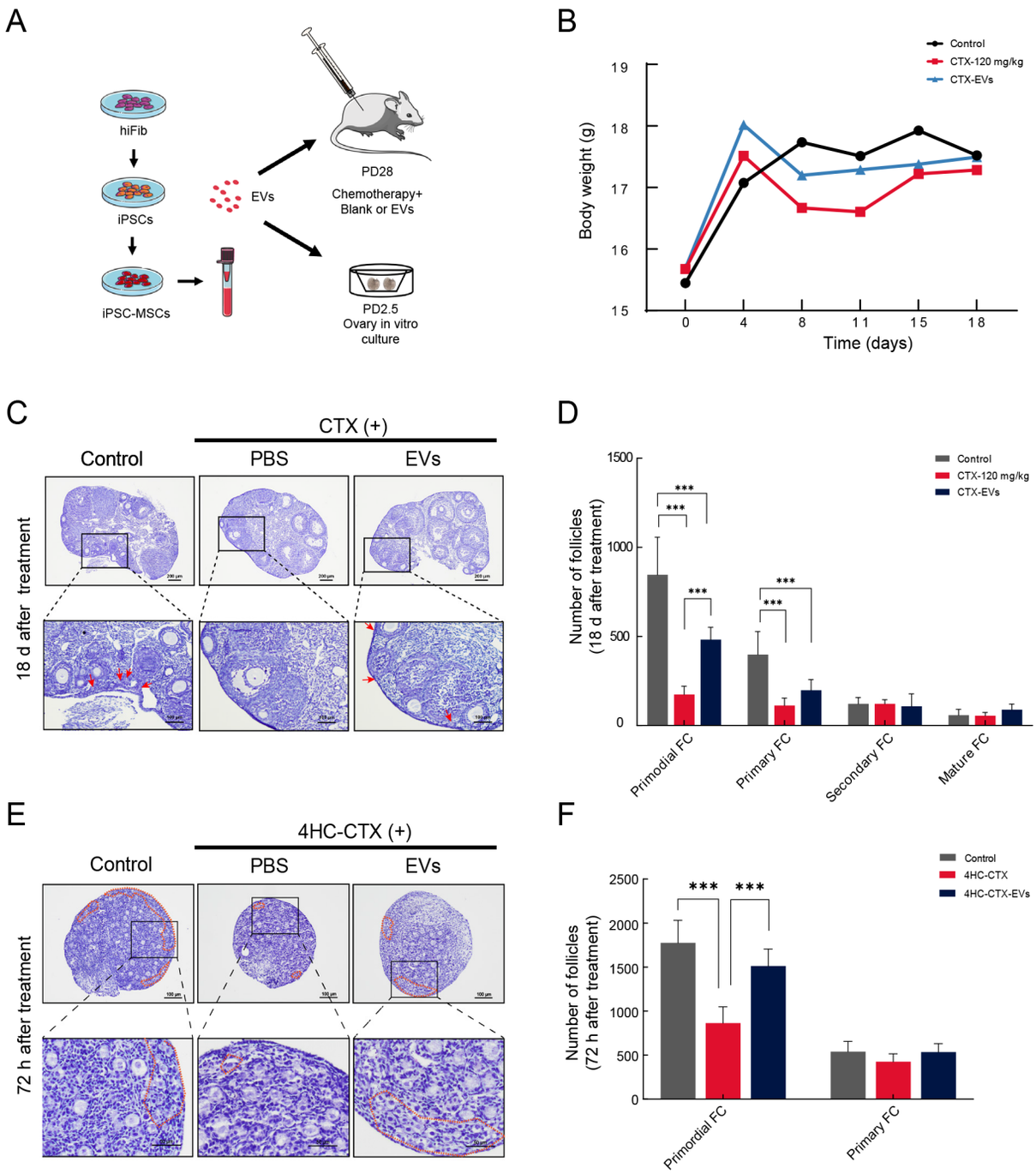

Figure 2 iPSC-MSC-EVs protected follicular development from chemotherapy-induced ovarian damage *in vivo* and *in vitro*

A: Schematic of experimental procedure of iPSC-MSC-EV isolation and animal experiments. B: Body weight of different groups at 0, 4, 8, 11, 15, and 18 days are displayed on weight curve. C: Hematoxylin staining of follicle morphology at various stages in different treatment groups after chemotherapy (CTX 120 mg/kg) and iPSC-MSC-EV transplantation (200 μg) in adult ovary. Red arrow indicates primordial follicles. D: Columns display total number of primordial, primary, secondary, and mature follicles in different groups (n=6). Quantification of ovarian follicles showed statistically significant reduction in number of primordial and primary follicles between CTX and control groups. After iPSC-MSC-EV transplantation, primordial follicle number was significantly higher than that in CTX group. E: Ovaries from PD2–PD3 mice were cultured *in vitro* with 4HC-CTX (10 μmol/L) with or without iPSC-MSC-EVs (100 μg/mL) for 72 h, followed by histological analysis with hematoxylin staining. Primordial follicles are highlighted by a broken orange line. F: Columns display total number of primordial and primary follicles in different groups of *in vitro*-cultured ovaries (n=4). Number of primordial follicles in 4HC-CTX treated group was significantly lower than that in control and 4HC-CTX-EV groups. For primary follicles, no significant differences were observed among groups. In all panels, data are mean±*SD*. *: P<0.05; **: P<0.01; ***: P<0.001.

After 24 h of incubation, cell viability was assessed using MTS reagent, revealing a significant decrease (P<0.01) in granulosa cell viability in the CTX (2 mg/mL) group compared to the control group.

However, the simultaneous administration of iPSC-MSC-EVs at varying doses (2, 10, or 20 μg/mL) resulted in a significant dose-dependent increase in granulosa cell viability (P<0.05), with 20 μg/mL iPSC-MSC-EVs exhibiting the strongest positive effect (Figure 3C). Treatment with 4 mg/mL CTX significantly decreased granulosa cell viability (P<0.001),

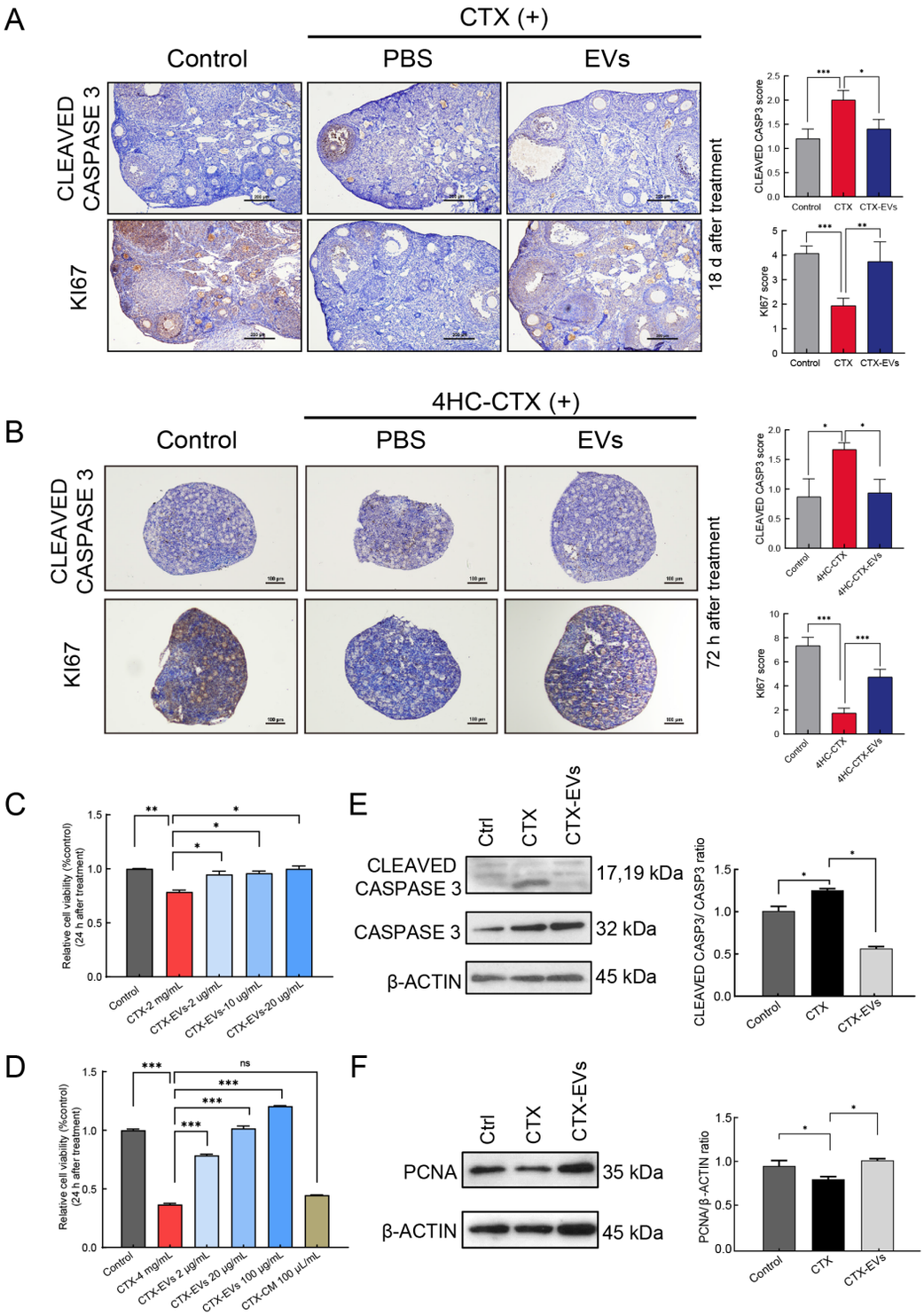

Figure 3 iPSC-MSC-EVs protected against chemotherapy-induced ovarian damage by inhibiting granulosa cell apoptosis and improving proliferation

A: Detection of cell apoptosis marker CLEAVED CASPASE 3 and cell proliferation marker KI67 by IHC staining in adult ovaries. IHC staining scores were analyzed statistically (right panel). Scale bar: 200 μm. B: Detection of cell apoptosis marker CLEAVED CASPASE 3 and cell proliferation marker KI67 by IHC staining in cultured ovaries. IHC staining scores were analyzed statistically (right panel). Scale bar: 100 μm. C: Granulosa cell viability after treatment with CTX (2 mg/mL) and iPSC-MSC-EVs (2, 10, 20 μg/mL), measured by MTS assay (*n*=3). D: Granulosa cell viability after treatment with CTX (4 mg/mL) and iPSC-MSC-EVs (2, 20, 100 μg/mL) or iPSC-MSC-EV CM (condition medium), measured by MTS assay (*n*=3). Results showed that iPSC-MSC-EVs dramatically improved cell survival in a dose-dependent manner compared to CTX treated group. E: Expression levels of CASPASE 3 and CLEAVED CASPASE 3 in control, CTX (2 mg/mL), and CTX plus iPSC-MSC-EV (20 μg/mL) co-treated granulosa cells, detected by western blotting. β-actin was used as an internal control. Protein expression levels were quantified by Image J (right panel). F: Expression levels of PCNA in control, CTX (2 mg/mL), and CTX plus iPSC-MSC-EV co-treated granulosa cells, detected by western blotting. β-actin was used as an internal control. Protein expression levels were quantified by ImageJ (right panel). In all panels, data mean±*SD*. *: $P<0.05$; **: $P<0.01$; ***: $P<0.001$.

while co-treatment with iPSC-MSC-EVs restored viability in a dose-dependent manner (P<0.001), although treatment with iPSC-MSCs CM did not (Figure 3D). These results suggest that iPSC-MSC-EVs can significantly improve the survival of CTX-injured granulosa cells *in vitro*.

Western blot analysis of the expression of apoptosis- and proliferation-related markers in CTX-treated, CTX-EV-treated, and untreated granulosa cells *in vitro* showed that the ratio of CLEAVED CASPASE 3 to CASPASE 3, a common indicator of apoptotic state, was significantly elevated under CTX treatment. However, this increase in granulosa cell apoptosis was significantly reversed in the CTX-EV treatment group (Figure 3E). Western blot analysis of cell proliferation marker PCNA showed that expression was significantly lower in the CTX group, but higher in the CTX-EV group, further indicating that iPSC-MSC-EVs can promote granulosa cell proliferation (Figure 3F) and may protect ovaries from injury by attenuating chemotherapy-induced apoptosis and promoting proliferation of granulosa cells.

iPSC-MSC-EVs reversed CTX-induced down-regulation of ILK pathway, possibly by transferring functional miRNAs

To further investigate the molecular mechanism by which iPSC-MSC-EVs protect granulosa cells, we conducted RNA-seq to define transcriptomic changes associated with the EVs. Based on the analysis of differentially expressed genes (DEGs) between CTX-treated and untreated granulosa cells in mice, we identified 428 DEGs, including 112 significantly up-regulated and 316 significantly down-regulated DEGs, in the CTX-treated group (|Log2 (fold-change)| >1 and P<0.05). Comparison between CTX-treated and CTX-EV-treated granulosa cells identified 1 451 DEGs, including 587 up-regulated DEGs and 864 down-regulated DEGs, in the CTX-EV-treated group (Figure 4A).

KEGG analysis showed that DEGs in the CTX-EV group were mainly enriched in pathways related to signal transduction and cell metabolism (Figure 4B). Analysis of these DEGs and IPA predictions of the top 10 most significantly affected pathways revealed that the ILK signaling pathway was inhibited under CTX treatment but reactivated under CTX-EV co-treatment (Figure 4C). Subsequent screening of the top 1 000 genes using Qlucore, based on log (fold-change)>1.5 and highest P-value (Supplementary Figure S3A), followed by IPA, indicated that the ILK signaling pathway was ranked fourth among the 10 most significantly affected pathways (Supplementary Figure S3B). Heatmap visualization of the ILK pathway-related DEGs confirmed that they were down-regulated in the CTX group compared with the control group (Figure 4D) but up-regulated in the CTX-EV-treated granulosa cells.

QRT-PCR analysis confirmed that ILK-related gene expression (i.e., *Ilk*, *Pten*, *Krt18*, *Ccnd1*, *Cdkn 2a*, and *Vegfa*) was generally consistent with the sequencing results (Figure 4E). Specifically, qRT-PCR showed that *Ptgs2*, which contributes to cumulus granulosa cell survival during expansion (Guo et al., 2016), was reduced in the CTX-treated granulosa cells compared with the untreated cells but was significantly up-regulated under CTX-EV treatment (P<0.05). In contrast, expression of the apoptotic gene *Bax* was significantly increased in the CTX group (P<0.05) but significantly decreased in the CTX-EV group (P<0.05). The anti-apoptotic gene *Bcl2* did not differ significantly among treatment groups. These results suggest that iPSC-MSC-EVs can protect granulosa cells from apoptosis and maintain normal function via regulation of the ILK signaling pathway.

EVs secreted by MSCs can exert regenerative effects on damaged tissues by transferring functional miRNAs (Ranghino et al., 2017; Sun et al., 2019). Here, MTS assay demonstrated that RNase-treated EVs failed to up-regulate granulosa cell viability compared to the untreated EVs (Supplementary Figure S3C), indicating that RNA in the iPSC-MSC-EVs may have a therapeutic effect on chemotherapy-induced granulosa cell damage. Therefore, based on high-throughput miRNA sequencing, we identified the top 50 miRNAs expressed in iPSC-MSC-EVs (Figure 4F). Nine of the top 50 miRNAs were predicted to target PTEN (Figure 4G), a lipid phosphatase that negatively regulates ILK activation (Attwell et al., 2003; Im & Dagnino, 2018; Persad et al., 2000). Thus, miRNAs in iPSC-MSC-EVs may up-regulate the expression of ILK by down-regulating the expression of PTEN. GO enrichment analysis revealed that the top 50 miRNA-targeted genes were enriched in the neuronal ribonucleoprotein granule and checkpoint clamp complex (Figure 4H). DIANA-miRPath pathway enrichment analysis showed that pathways collectively targeted by the top 50 miRNAs were mainly enriched in the extracellular matrix (ECM)-receptor interaction pathway, signaling pathways regulating stem cell pluripotency, and mucin-type O-glycan biosynthesis (Figure 4I).

Taken together, these results suggest that iPSC-MSC-EVs may reverse CTX-induced down-regulation of the ILK pathway in granulosa cells, possibly by transferring functional miRNAs.

iPSC-MSC-EVs reversed CTX-induced down-regulation of PTEN/ILK/AKT pathway *in vivo* and *in vitro*

ILK is a key protein that links integrins to the cytoskeleton and exhibits serine and threonine protein kinase activity (Górska & Mazur, 2022). In particular, ILK can phosphorylate AKT on Ser473 to regulate proliferation, migration, and other cellular functions (Acconcia et al., 2007; Wu & Dedhar, 2001). ILK also participates in other cellular processes, such as regulation of the G1/S/G2 phase of the cell cycle, cell migration and adhesion, and inhibition of apoptosis (Attwell et al., 2003; Radeva et al., 1997).

Western blot detection of ILK pathway protein expression in the granulosa cells showed that PTEN expression was significantly up-regulated after CTX treatment but was suppressed in the presence of iPSC-MSC-EVs. In contrast, ILK expression was significantly reduced after CTX treatment but was increased after the addition of iPSC-MSC-EVs. In addition, the p-AKT/AKT ratio was significantly decreased after CTX treatment but ameliorated following exposure to iPSC-MSC-EVs. Thus, while CTX treatment inhibited the ILK/AKT pathway via up-regulation of PTEN, exposure to iPSC-MSC-EVs reversed this effect (Figure 5A). In contrast, the RNase-treated iPSC-MSC-EVs had no such effect (Supplementary Figure S3D).

We also examined the regulatory effects of iPSC-MSC-EVs on cell cycle-related proteins CCNB1, CCND1, and P27. Western blotting revealed that P27 expression was significantly increased after addition of chemotherapeutic agents but decreased after treatment with iPSC-MSC-EVs. CCND1 expression was significantly decreased under CTX treatment but was restored by iPSC-MSC-EVs. In contrast, CCNB1 expression was not significantly affected by the presence of either CTX or iPSC-MSC-EVs (Figure 5B).

Western blot analysis of ILK pathway expression in cultured

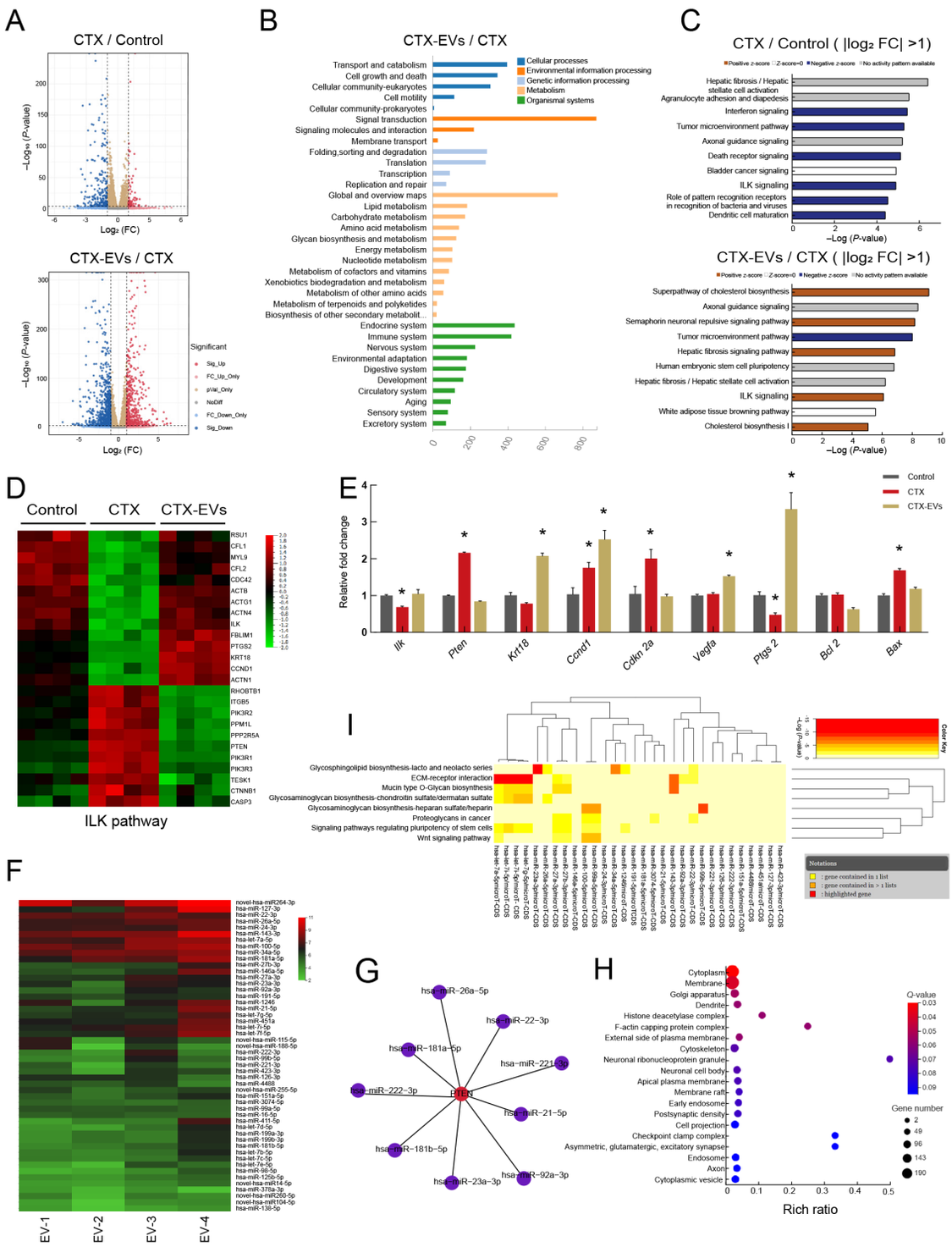

Figure 4 Analysis of RNA-seq data from granulosa cells and miRNA-seq data from iPSC-MSC-EVs

A: Volcano plots comparing DEGs in different groups. Red points represent up-regulated genes, blue points represent down-regulated genes. |Log_2 (fold-change)|=1 and *P*=0.01 are marked by black broken lines. B: KEGG analysis of genes from five clusters enriched in biological process terms. C: Analysis of DEGs (|log2 fold-change|>1) between CTX and control groups using IPA. Top 10 affected pathways are shown. Analysis of DEGs (|log_2 (fold-change)|>1) between CTX-EV and CTX groups using IPA. Top 10 affected pathways are shown. IPA indicated that ILK signaling pathway was down-regulated in CTX-treated group compared to control group. However, ILK signaling pathway was up-regulated in CTX-EV group compared to CTX group. D: Heatmap of relative gene expression levels of DEGs related to ILK pathway. E: qRT-PCR results of expression of ILK pathway-related genes (*Ilk*, *Pten*, *Krt18*, *Ccnd1*, *Cdkn2a*, and *Vegfa*), cumulus expansion-related genes (*Ptgs2*), and apoptosis marker genes (*Bcl2*, *Bax*) in granulosa cells. Data are represented as mean±*SD*. *: *P*<0.05. F: Top 50 miRNAs expressed in iPSC-MSC-EVs from biological replicate samples detected by miRNA sequencing. G: Nine of the top 50 miRNAs were predicted to target PTEN by miRWalk and miRTarBase analysis. H: GO enrichment analysis of genes targeted by top 50 miRNAs in iPSC-MSC-EVs. I: Significant KEGG pathways collectively targeted by top 50 miRNAs analyzed by DIANA-miRPath v3.0 (*P*<0.05). Attached dendrograms on two axes represent hierarchical clustering results for miRNAs and pathways, respectively.

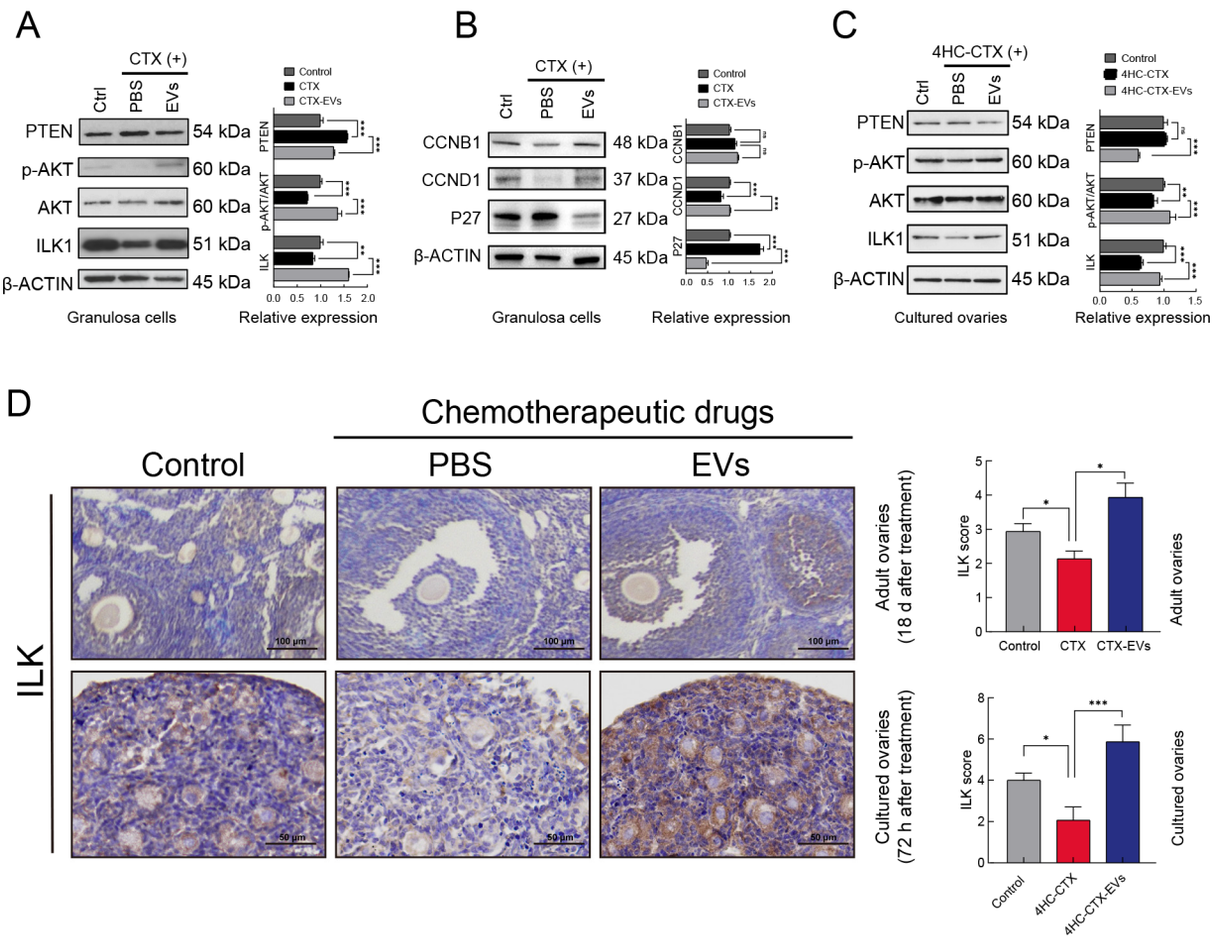

Figure 5 iPSC-MSC-EVs reversed CTX-induced down-regulation of PTEN/ILK/AKT pathway in *in vivo* and *in vitro*

A: Western blot analysis of expression of ILK, AKT, phosphorylated AKT (Ser 473), and PTEN in untreated, CTX (2 mg/mL) treated, and CTX plus iPSC-MSC-EV (20 μg/mL) co-treated granulosa cells. Quantitative protein analysis was performed by ImageJ (right panel). B: Western blot analysis of expression of cell cycle-related proteins CCNB1, CCND1, and P27 in untreated, CTX (2 mg/mL) treated, and CTX plus iPSC-MSC-EV (20 μg/mL) co-treated granulosa cells. Quantitative protein analysis was performed by ImageJ (right panel). C: Western blot analysis of expression of ILK, AKT, phosphorylated AKT (Ser 473), and PTEN in control, 4HC-CTX (10 μmmol/L) treated, and 4HC-CTX plus iPSC-MSC-EV (100 μg/mL) co-treated *in vitro*-cultured ovaries of mice. Quantitative protein analysis was performed by ImageJ (right panel). D: IHC staining showed that ILK expression was decreased in chemotherapy-treated group but increased after iPSC-MSC-EV transplantation in adult and *in vitro*-cultured ovaries. IHC staining scores were analyzed statistically (right panel). Scale bar: 200 μm, 50 μm respectively. In all panels, data are mean±*SD*. *: $P<0.05$; **: $P<0.01$; ***: $P<0.001$.

ovaries showed that PTEN expression was not significantly altered by CTX treatment but was significantly reduced following the addition of iPSC-MSC-EVs. ILK expression in the cultured ovaries was significantly inhibited under CTX treatment but rescued by the addition of iPSC-MSC-EVs, consistent with our results above. The P-AKT/AKT ratio also decreased significantly upon addition of CTX but reversed in the presence of iPSC-MSC-EVs (Figure 5C). Furthermore, IHC detection of ILK expression in adult mouse ovaries and *in vitro*-cultured ovaries showed that ILK expression was inhibited by CTX treatment but rescued by iPSC-MSC-EV exposure (Figure 5D). These cumulative results indicate that iPSC-MSC-EVs can reverse CTX-induced down-regulation of the PTEN/ILK/AKT pathway in mouse ovaries both *in vivo* and *in vitro*.

iPSC-MSC-EVs alleviated chemotherapy-induced ovarian injury via ILK/AKT pathway up-regulation

ILK plays an important role in protecting against radiotherapy-induced cellular injury, although (Hehlgans et al., 2007) the role of ILK in chemotherapy has not been explicitly characterized. To investigate whether iPSC-MSC-EVs protect against chemotherapy-induced ovarian injury by modulating the ILK/AKT pathway, we investigated the role of ILK in granulosa cells. We first overexpressed ILK using a lentivirus vector to infect granulosa cells. The granulosa cells were divided into lentivirus vector control and ILK overexpression (LV-ILK) groups. Western blot analysis confirmed that ILK expression was significantly increased in the LV-ILK group compared to the vector control group, and the p-AKT/AKT ratio was also significantly increased under ILK overexpression, implying that ILK regulates AKT phosphorylation in granulosa cells (Figure 6A). Subsequent examination of cell cycle-related proteins CCNB1, CCND1, and P27 revealed that P27 expression was significantly decreased, CCND1 expression was increased, and CCNB1 expression was unaffected in the LV-ILK group compared to the control (Figure 6B).

To test w hether ILK up-regulation protects against chemotherapy-induced apoptosis, CTX (2 mg/mL) was administered to vector and LV-ILK granulosa cells. MTS assay showed that cell viability was significantly lower in the vector

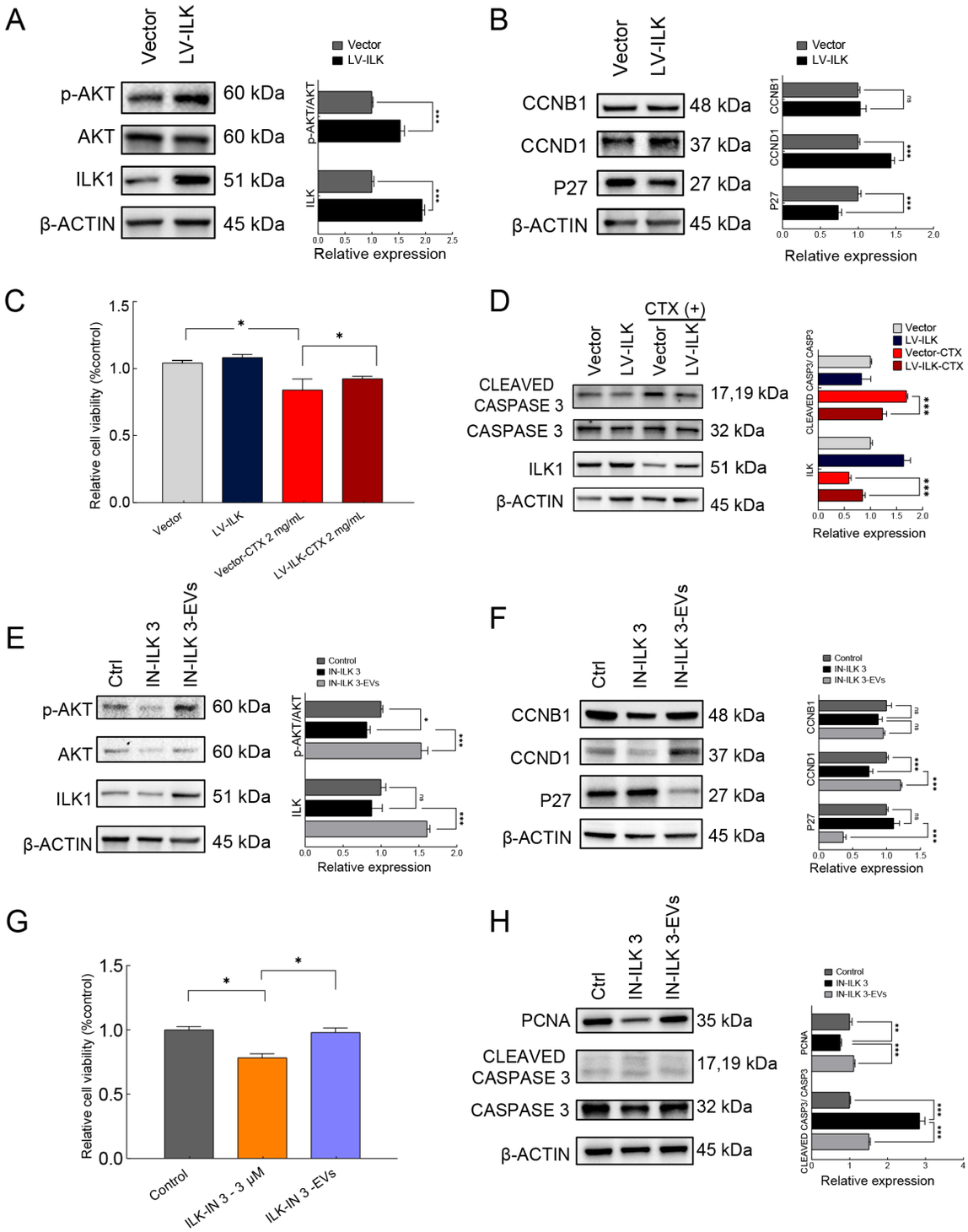

Figure 6 iPSC-MSC-EVs alleviated chemotherapy-induced ovarian injury through up-regulation of ILK/AKT pathway

A: Expression levels of ILK, AKT, and phosphorylated AKT (Ser 473) in vector control and ILK overexpression (LV-ILK) groups detected by western blot analysis. Protein expression levels were quantified by ImageJ (right panel). B: Expression levels of cell cycle-related proteins P27, CCNB1, and CCND1 in vector control and LV-ILK groups detected by western blot analysis. Protein expression levels were quantified by ImageJ (right panel). C: Granulosa cell viability in vector group and ILK overexpression group (LV-ILK) treated with or without CTX (2 mg/mL), determined by MTS assay (*n*=3). D: Expression of CLEAVED CASPASE3 and CASPASE3 in vector, LV-ILK, CTX-treated vector, and CTX-treated LV-ILK groups detected by western blot analysis. Protein expression levels were quantified by ImageJ (right panel). E: Western blot analysis of expression of ILK, AKT, and phosphorylated AKT (Ser473) in control, ILK inhibitor ILK-IN3 (10 μmol/L) treated, and ILK-IN3 plus EV (20 μg/mL) co-treated granulosa cells. Protein expression levels were quantified by ImageJ (right panel). F: Western blot analysis of expression of cell cycle-related proteins P27, CCNB1, and CCND1 in control, ILK-IN3 (10 μmol/L), and ILK-IN3-EV groups. Protein expression levels were quantified by ImageJ (right panel). G: Granulosa cell viability in control, ILK-IN3 (10 μmol/L), and ILK-IN3-EV groups, determined by MTS assay (*n*=3). H: Western blot analysis of expression of PCNA, CLEAVED CASPASE3, and CASPASE3 in control, ILK-IN3 (10 μmol/L), and ILK-IN3-EV groups. Protein expression levels were quantified by ImageJ (right panel). In all panels, data are represented as mean±*SD*. *: *P*<0.05; **: *P*<0.01; ***: *P*<0.001.

group after treatment with CTX (P<0.05) (Figure 6C). Although cell viability was also decreased in the CTX-treated LV-ILK granulosa cells, it was significantly higher than that in the CTX-treated vector group (Figure 6C). Western blot analysis of apoptosis-related gene expression, i.e., CLEAVED CASPASE 3 and CASPASE 3, revealed that overexpression of ILK resulted in suppression of the CLEAVED CASPASE 3/CASPASE 3 ratio, which was up-regulated by CTX treatment (Figure 6D). These results imply that ILK overexpression confers inhibitory effects on CTX-induced apoptosis in granulosa cells.

To test the effects of attenuated ILK pathway signaling, we treated cultured granulosa cells with the ILK-specific competitive inhibitor (Eke et al., 2009; Wang et al., 2011; Younes et al., 2007) ILK-IN3 (10 μmol/L) and detected changes in protein levels after 48 h. Western blotting showed no significant changes in ILK expression after the addition of ILK-IN3, although the p-AKT/AKT ratio was significantly decreased, indicating that ILK-IN3 inhibited ILK phosphorylation of AKT. However, both ILK expression and the p-AKT/AKT ratio were significantly increased in the presence of iPSC-MSC-EVs, indicating that the effects of ILK-IN3 were reversed and the AKT pathway was activated via iPSC-MSC-EV-induced up-regulation of ILK (Figure 6E). Detection of cell cycle-related proteins indicated that CCNB1 expression was not affected, CCND1 expression was significantly decreased, and P27 expression was significantly increased in the ILK-IN3-treated group, with these effects reversed by iPSC-MSC-EV treatment (Figure 6F).

MTS-based quantification of the control, ILK-IN3 (10 μmol/L)-treated, and ILK-IN3/iPSC-MSC-EV-co-treated groups confirmed that granulosa cell viability was significantly decreased in the presence of ILK-IN3 (P<0.05), while the increase in apoptotic cells was reversed by simultaneous addition of iPSC-MSC-EVs (Figure 6G). Western blot analysis showed that the CLEAVED CASPASE 3 to CASPASE 3 ratio increased significantly after the addition of ILK-IN3, but this increasing trend was rescued by iPSC-MSC-EV treatment. The expression of PCNA was significantly down-regulated in granulosa cells exposed to ILK-IN 3, but expression levels were restored by the addition of iPSC-MSC-EVs (Figure 6H). These results imply that inhibition of ILK function promotes apoptosis and inhibits proliferation of granulosa cells, while exposure to iPSC-MSC-EVs promotes ILK expression, thereby reversing the deleterious effects on granulosa cells. Taken together, these results suggest that iPSC-MSC-EVs can limit chemotherapy-induced injury through positive regulation of the ILK/AKT pathway.

DISCUSSION

EVs secreted by MSCs from various sources such as bone marrow (Yang et al., 2020), adipose tissue (Huang et al., 2018), and human amnion (Ding et al., 2020a) can exert therapeutic effects on ovarian tissue damage and ovarian aging. In addition, EVs secreted by iPSC-MSCs can reduce osteoporosis (Qi et al., 2016), promote wound healing (Zhang et al., 2015), and alleviate limb ischemia (Hu et al., 2015) by inhibiting cell apoptosis and promoting angiogenesis. Studies have also shown that iPSC-MSC-EVs can inhibit ECM deposition, resulting in corneal repair (Tang et al., 2022). Our study provides the first description of the therapeutic effects of iPSC-MSC-EVs in chemotherapy-induced ovarian damage. We found that iPSC-MSC-EVs can ameliorate the induction of apoptosis in granulosa cells and promote their proliferation, presumably by transferring regulatory miRNAs that activate the ILK/AKT pathway, thereby protecting against ovarian damage (Figure 7).

As a commonly used chemotherapeutic drug, CTX treatment can be accompanied by strong reproductive toxicity, menstrual disorders, amenorrhea, and infertility in female cancer patients (Dann et al., 2005). CTX can cause premature ovarian insufficiency by the induction of granulosa cell apoptosis, rapid follicular reserve depletion, microvascular damage, and ovarian tissue fibrosis and necrosis (Ding et al., 2020b). In addition, follicular atresia may also occur when >10% of granulosa cells undergo apoptosis (Fu et al., 2008). In this study, we used CTX as a chemotherapeutic agent to induce ovarian damage in mice. Histological morphology, follicle counts, and body weight measurements in mice with CTX-induced ovarian damage showed that iPSC-MSC-EV treatment reversed the significant reduction in normal follicle counts, especially primordial follicles, and reversed the increase in apoptosis caused by CTX in both ovarian granulosa cells and cultured mouse ovaries. Previous research has shown that co-culture of granulosa cells with human umbilical cord mesenchymal stem cells (hUCMSCs)-secreted EVs promotes cell proliferation and resistance to cisplatin-induced damage (Sun et al., 2017). EVs derived from human amniotic epithelial cells (hAECs) can also inhibit chemotherapy-induced apoptosis in granulosa cells (Zhang et al., 2019). Our study showed that iPSC-MSC-EVs can inhibit the chemotherapy-induced decrease in granulosa cells in *in vitro* culture.

The AKT pathway downstream of ILK is essential for folliculogenesis, and its disruption impairs primordial follicle survival, leading to the occurrence of POI (Kalich-Philosoph et al., 2013; Wang et al., 2019). Here, granulosa cell transcriptome sequencing revealed significantly higher ILK pathway expression in cells treated with iPSC-MSC-EVs and CTX than with CTX alone. Western blot and IHC analysis showed that ILK protein expression was up-regulated, PI3K/AKT pathway was activated, cell cycle activation protein CCND 1 was up-regulated, and cell cycle inhibitory protein p27 was down-regulated after iPSC-MSC-EV treatment.

Studies have found that EVs from MSCs can transfer functional miRNAs to target cells to regulate their function, resulting in therapeutic effects in damaged ovarian tissue. For example, miR-644-5p in stem cells improves ovarian function in rats with chemotherapy-induced ovarian damage by targeting P53 (Sun et al., 2019). Similarly, EVs secreted by human amniotic membrane-derived mesenchymal stromal cells (hAMSCs) release miRNA-320a, which regulates SIRT4 to protect against ovarian oxidative stress in mice with POI (Ding et al., 2020a). In addition, miRNA-17-5p derived from human umbilical cord MSCs improves ovarian function after chemotherapy by regulating SIRT7 (Ding et al., 2020b).

In this study, iPSC-MSC-EVs inhibited CTX-induced granulosa cell apoptosis and up-regulation of the ILK-PI3K/AKT pathway, which were abolished after EV-containing RNA was degraded by RNase. This suggested that the regenerative effects of iPSC-MSC-EVs may be exerted through the transfer of functional miRNAs. Here, miRNA sequencing revealed that iPSC-MSC-EVs contained multiple miRNAs predicted to target the ILK negative regulator PTEN. Western blot and qRT-PCR analysis showed that the expression of PTEN was decreased after iPSC-MSC-EV treatment in granulosa cells and cultured ovaries. Previous

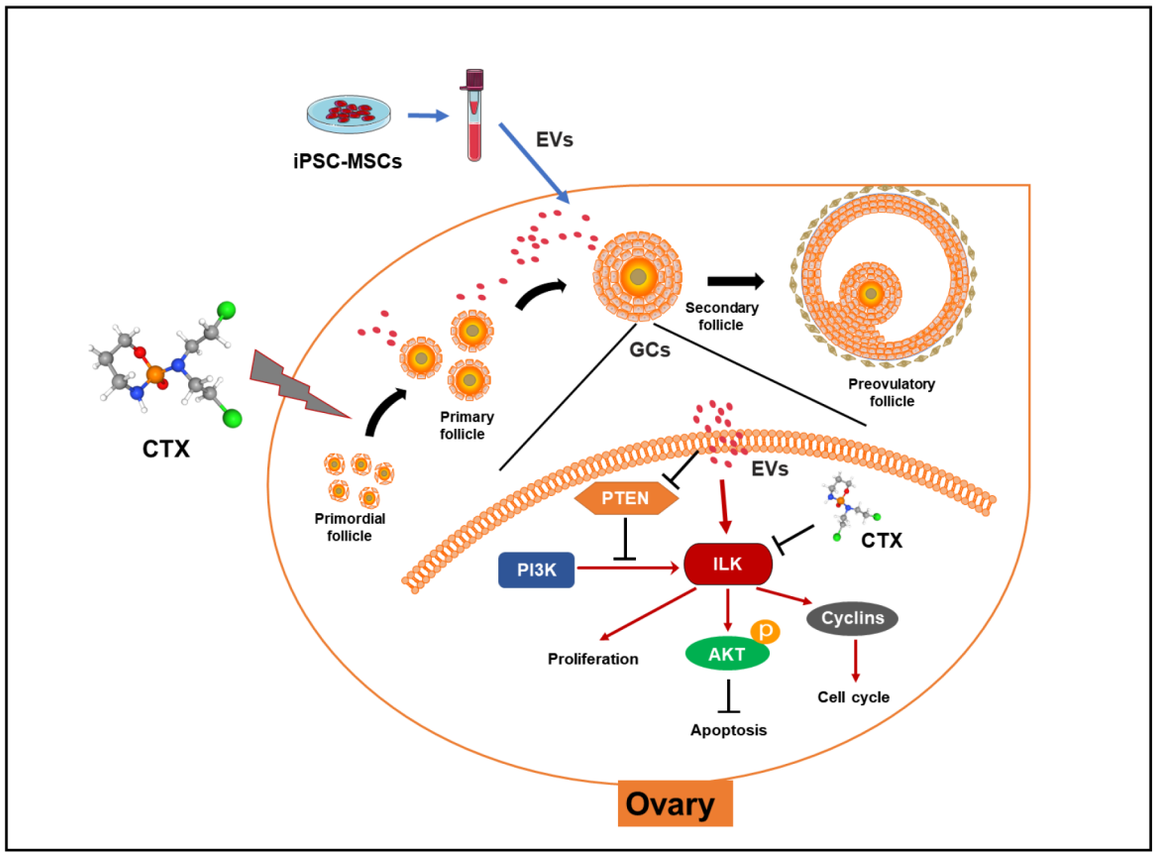

Figure 7 Molecular mechanisms by which iPSC-MSC-EVs attenuate chemotherapy-induced ovarian damage

EVs secreted by iPSC-MSCs carrying functional miRNAs reversed CTX-induced down-regulation of ILK-PI3K/AKT pathway in granulosa cells, thereby promoting their proliferation and inhibiting their apoptosis.

study has shown that exosomes produced by bone marrow MSCs can target PTEN by delivering mir-144-5p, thereby improving ovarian function in rats after chemotherapy-induced ovarian insufficiency (Yang et al., 2020). Bioinformatics analysis showed that the pathways collectively targeted by the top 50 miRNAs were enriched in the ECM-receptor interaction pathway. ILK is a downstream component of ECM-integrin signaling (Broekmans et al., 2007; Kang et al., 2016). As iPSC-MSC-EVs contained multiple miRNAs targeting the ECM-receptor interaction pathway, it is difficult to determine which plays a dominant role, and thus the mechanisms of miRNA interactions with the ECM-receptor interaction pathway and ILK expression require further investigation.

The role of the ILK pathway in granulosa cells is currently unclear. Our results showed that overexpression of ILK in granulosa cells activated the AKT pathway and inhibited chemotherapy-induced decline in cell number. Inhibition of ILK protein function by ILK-IN3 resulted in decreased levels of phosphorylated AKT, increased cell apoptosis, decreased cell proliferation, and significantly reduced granulosa cell viability. However, the addition of EVs restored ILK expression, along with p-AKT levels, indicating that iPSC-MSC-EVs promote ILK expression in granulosa cells, which, in turn, enhances AKT phosphorylation.

This study has several limitations. First, although EV treatment successfully alleviated ovarian damage in mice, more fertility markers need to be tested. Second, we did not identify which specific miRNAs in iPSC-MSC-EVs are essential for the beneficial effects on ovarian injury. Thus, the effects of EV-associated miRNAs in the ovary and safety of iPSC-MSC-EVs need to be explored regarding potential clinical use. Overall, we demonstrated that EVs secreted by iPSC-MSCs can limit chemotherapy-induced ovarian damage in mice and elucidated the underlying molecular mechanisms. The current study provides a promising technique for the clinical treatment of chemotherapy-induced premature ovarian insufficiency and lays a foundation for the clinical application of iPSC-MSC-secreted EVs.

DATA AVAILABILITY

The raw RNA-seq data were deposited in the NCBI Sequence Read Archive (SRA) (BioProjectID PRJNA916119), GSA Database (Accession No. CRA009327), and Science Data Bank (DOI:10.57760/sciencedb.j00139.00048). The raw miRNA-seq data were deposited in the NCBI SRA (BioProjectID PRJNA915756), GSA Database (Accession No. HRA003686), and Science Data Bank (DOI 10.57760/sciencedb.j00139.00047).

SUPPLEMENTARY DATA

Supplementary data to this article can be found online.

COMPETING INTERESTS

The authors declare that they have no competing interests.

AUTHORS' CONTRIBUTIONS

W.Y.C., J.L.M., G.L., and R.C.C. contributed to project conception. J.L.M., G.L., H.B.L., and W.Y.C. contributed to funding acquisition. R.-C.C. conducted experiments. Y.L., R.C.C, X.W.S., and Z.Q.X. analyzed data and prepared the figures and manuscript. W.M.W., C.L.T., and Y.L. provided technical support. All authors read and approved the final version of the manuscript.

ACKNOWLEDGMENTS

We thank Li-Hong Wang, Xiao-Hua Luan, Zai-Xin Zhang, and the R&D Team of SDU-CUHK for help with animal and histological experiments.

REFERENCES

Acconcia F, Barnes CJ, Singh RR, et al. 2007. Phosphorylation-dependent regulation of nuclear localization and functions of integrin-linked kinase. *Proceedings of the National Academy of Sciences of the United States of America*, **104**(16): 6782−6787.

Attwell S, Mills J, Troussard A, et al. 2003. Integration of cell attachment, cytoskeletal localization, and signaling by integrin-linked kinase (ILK), CH-ILKBP, and the tumor suppressor PTEN. *Molecular Biology of the Cell*, **14**(12): 4813−4825.

Basu J, Ludlow JW. 2016. Exosomes for repair, regeneration and rejuvenation. *Expert Opinion on Biological Therapy*, **16**(4): 489−506.

Broekmans FJ, Knauff EAH, Te Velde ER, et al. 2007. Female reproductive ageing: current knowledge and future trends. *Trends in Endocrinology & Metabolism*, **18**(2): 58−65.

Coulam CB, Adamson SC, Annegers JF. 1986. Incidence of premature ovarian failure. *Obstetrics and Gynecology*, **67**(4): 604−606.

Dann EJ, Epelbaum R, Avivi I, et al. 2005. Fertility and ovarian function are preserved in women treated with an intensified regimen of cyclophosphamide, adriamycin, vincristine and prednisone (Mega-CHOP) for non-Hodgkin lymphoma. *Human Reproduction*, **20**(8): 2247−2249.

Desmeules P, Devine PJ. 2006. Characterizing the ovotoxicity of cyclophosphamide metabolites on cultured mouse ovaries. *Toxicological Sciences*, **90**(2): 500−509.

Ding CY, Qian CF, Hou SY, et al. 2020a. Exosomal miRNA-320a is released from hAMSCs and regulates SIRT4 to prevent reactive oxygen species generation in POI. *Molecular Therapy Nucleic Acids*, **21**: 37−50.

Ding CY, Zhu LP, Shen H, et al. 2020b. Exosomal miRNA-17–5p derived from human umbilical cord mesenchymal stem cells improves ovarian function in premature ovarian insufficiency by regulating SIRT7. *Stem Cells*, **38**(9): 1137−1148.

Dominici M, Le Blanc K, Mueller I, et al. 2006. Minimal criteria for defining multipotent mesenchymal stromal cells. The international society for cellular therapy position statement. *Cytotherapy*, **8**(4): 315−317.

Eke I, Leonhardt F, Storch K, et al. 2009. The small molecule inhibitor QLT0267 Radiosensitizes squamous cell carcinoma cells of the head and neck. *PLoS One*, **4**(7): e6434.

Fang CC, Chou TH, Huang JW, et al. 2018. The small molecule inhibitor QLT-0267 decreases the production of fibrin-induced inflammatory cytokines and prevents post-surgical peritoneal adhesions. *Scientific Reports*, **8**(1): 9481.

Fu X, He Y, Xie C, et al. 2008. Bone marrow mesenchymal stem cell transplantation improves ovarian function and structure in rats with chemotherapy-induced ovarian damage. *Cytotherapy*, **10**(4): 353−363.

Górska A, Mazur AJ. 2022. Integrin-linked kinase (ILK): the known vs. the unknown and perspectives. *Cellular and Molecular Life Sciences:CMLS*, **79**(2): 100.

Guo J, Shi LY, Gong XH, et al. 2016. Oocyte-dependent activation of MTOR in cumulus cells controls the development and survival of cumulus-oocyte complexes. *Journal of Cell Science*, **129**(16): 3091−3103.

Harrell CR, Jovicic N, Djonov V, et al. 2019. Mesenchymal stem cell-derived exosomes and other extracellular vesicles as new remedies in the therapy of inflammatory diseases. *Cells*, **8**(12): 1605.

Hehlgans S, Eke I, Cordes N. 2007. An essential role of integrin-linked kinase in the cellular radiosensitivity of normal fibroblasts during the process of cell adhesion and spreading. *International Journal of Radiation Biology*, **83**(11–12): 769–779.

Helleday T, Petermann E, Lundin C, et al. 2008. DNA repair pathways as targets for cancer therapy. *Nature Reviews Cancer*, **8**(3): 193−204.

Hu GW, Li Q, Niu X, et al. 2015. Exosomes secreted by human-induced pluripotent stem cell-derived mesenchymal stem cells attenuate limb ischemia by promoting angiogenesis in mice. *Stem Cell Research & Therapy*, **6**(1): 10.

Huang BX, Lu JF, Ding CY, et al. 2018. Exosomes derived from human adipose mesenchymal stem cells improve ovary function of premature ovarian insufficiency by targeting SMAD. *Stem Cell Research & Therapy*, **9**(1): 216.

Im M, Dagnino L. 2018. Protective role of integrin-linked kinase against oxidative stress and in maintenance of genomic integrity. *Oncotarget*, **9**(17): 13637−13651.

Jankowska K. 2017. Premature ovarian failure. *Menopause Review/Przegląd Menopauzalny*, **16**(2): 51−56.

Jiao X, Ke HN, Qin YY, et al. 2018. Molecular genetics of premature ovarian insufficiency. *Trends in Endocrinology & Metabolism*, **29**(11): 795−807.

Jing H, He XM, Zheng JH. 2018. Exosomes and regenerative medicine: state of the art and perspectives. *Translational Research*, **196**: 1−16.

Kalich-Philosoph L, Roness H, Carmely A, et al. 2013. Cyclophosphamide triggers follicle activation and "burnout"; AS101 prevents follicle loss and preserves fertility. *Science Translational Medicine*, **5**(185): 185ra62.

Kang L, Mokshagundam S, Reuter B, Lark DS, Sneddon CC, Hennayake C, et al. 2016. Integrin-linked kinase in muscle is necessary for the development of insulin resistance in diet-induced obese mice. *Diabetes*, **65**(6): 1590−1600.

Krämer A, Green J, Pollard J Jr, et al. 2014. Causal analysis approaches in ingenuity pathway analysis. *Bioinformatics*, **30**(4): 523−530.

Liu XM, Zhang YL, Ji SY, et al. 2017. Mitochondrial function regulated by mitoguardin-1/2 is crucial for ovarian endocrine functions and ovulation. *Endocrinology*, **158**(11): 3988−3999.

Livak KJ, Schmittgen TD. 2001. Analysis of relative gene expression data using real-time quantitative PCR and the 2-ΔΔCT Method. *Methods*, **25**(4): 402−408.

Lobb RJ, Becker M, Wen SW, et al. 2015. Optimized exosome isolation protocol for cell culture supernatant and human plasma. *Journal of Extracellular Vesicles*, **4**(1): 27031.

Meirow D, Biederman H, Anderson RA, et al. 2010. Toxicity of chemotherapy and radiation on female reproduction. *Clinical Obstetrics and Gynecology*, **53**(4): 727−739.

Nagelkerke A, Ojansivu M, Van Der Koog L, et al. 2021. Extracellular vesicles for tissue repair and regeneration: evidence, challenges and opportunities. *Advanced Drug Delivery Reviews*, **175**: 113775.

Okita K, Matsumura Y, Sato Y, et al. 2011. A more efficient method to generate integration-free human iPS cells. *Nature Methods*, **8**(5): 409−412.

Okita K, Yamakawa T, Matsumura Y, et al. 2013. An efficient nonviral method to generate integration-free human-induced pluripotent stem cells from cord blood and peripheral blood cells. *Stem Cells*, **31**(3): 458−466.

Pedersen T, Peters H. 1968. Proposal for a classification of oocytes and follicles in the mouse ovary. *Reproduction*, **17**(3): 555−557.

Persad S, Attwell S, Gray V, et al. 2000. Inhibition of integrin-linked kinase (ILK) suppresses activation of protein kinase B/Akt and induces cell cycle arrest and apoptosis of PTEN-mutant prostate cancer cells. *Proceedings of the National Academy of Sciences of the United States of America*, **97**(7): 3207−3212.

Piasecka-Srader J, Blanco FF, Delman DH, et al. 2015. Tamoxifen prevents apoptosis and follicle loss from cyclophosphamide in cultured rat ovaries. *Biology of Reproduction*, **92**(5): 132.

Qi X, Zhang JY, Yuan H, et al. 2016. Exosomes secreted by human-induced pluripotent stem cell-derived mesenchymal stem cells repair critical-sized bone defects through enhanced angiogenesis and osteogenesis in osteoporotic rats. *International Journal of Biological*

Sciences, **12**(7): 836−849.

Qin YY, Jiao X, Simpson JL, et al. 2015. Genetics of primary ovarian insufficiency: new developments and opportunities. *Human Reproduction Update*, **21**(6): 787−808.

Radeva G, Petrocelli T, Behrend E, et al. 1997. Overexpression of the integrin-linked kinase promotes anchorage-independent cell cycle progression. *Journal of Biological Chemistry*, **272**(21): 13937−13944.

Ranghino A, Bruno S, Bussolati B, et al. 2017. The effects of glomerular and tubular renal progenitors and derived extracellular vesicles on recovery from acute kidney injury. *Stem Cell Research & Therapy*, **8**(1): 24.

Remmele W, Stegner HE. 1987. Recommendation for uniform definition of an immunoreactive score (IRS) for immunohistochemical estrogen receptor detection (ER-ICA) in breast cancer tissue. *Pathologe*, **8**(3): 138–140. (in German)

Sonigo C, Beau I, Binart N, et al. 2019. The impact of chemotherapy on the ovaries: molecular aspects and the prevention of ovarian damage. *International Journal of Molecular Sciences*, **20**(21): 5342.

Sun B, Ma YJ, Wang F, et al. 2019. miR-644–5p carried by bone mesenchymal stem cell-derived exosomes targets regulation of p53 to inhibit ovarian granulosa cell apoptosis. *Stem Cell Research & Therapy*, **10**(1): 360.

Sun LP, Li D, Song K, et al. 2017. Exosomes derived from human umbilical cord mesenchymal stem cells protect against cisplatin-induced ovarian granulosa cell stress and apoptosis *in vitro*. *Scientific Reports*, **7**(1): 2552.

Takahashi A, Yousif A, Hong LD, et al. 2021. Premature ovarian insufficiency: pathogenesis and therapeutic potential of mesenchymal stem cell. *Journal of Molecular Medicine*, **99**(5): 637−650.

Tang QM, Lu B, He J, et al. 2022. Exosomes-loaded thermosensitive hydrogels for corneal epithelium and stroma regeneration. *Biomaterials*, **280**: 121320.

Tang YY, Zhou Y, Li HJ. 2021. Advances in mesenchymal stem cell exosomes: a review. *Stem Cell Research & Therapy*, **12**(1): 71.

Vlachos IS, Zagganas K, Paraskevopoulou MD, et al. 2015. DIANA-miRPath v3.0: deciphering microRNA function with experimental support. *Nucleic Acids Research*, **43**(W1): W460−W466.

Wang W, Luo SM, Ma JY, et al. 2019. Cytotoxicity and DNA damage caused from diazinon exposure by inhibiting the PI3K-AKT pathway in porcine ovarian granulosa cells. *Journal of Agricultural and Food Chemistry*, **67**(1): 19−31.

Wang XF, Zhang ZQ, Yao C. 2011. Targeting integrin-linked kinase increases apoptosis and decreases invasion of myeloma cell lines and inhibits IL-6 and VEGF secretion from BMSCs. *Medical Oncology*, **28**(4): 1596−1600.

Wu CY, Dedhar S. 2001. Integrin-linked kinase (ILK) and its interactors: a new paradigm for the coupling of extracellular matrix to actin cytoskeleton and signaling complexes. *The Journal of Cell Biology*, **155**(4): 505−510.

Xia YG, Ling XZ, Hu GW, et al. 2020. Small extracellular vesicles secreted by human iPSC-derived MSC enhance angiogenesis through inhibiting STAT3-dependent autophagy in ischemic stroke. *Stem Cell Research & Therapy*, **11**(1): 313.

Yang ML, Lin L, Sha CL, et al. 2020. Bone marrow mesenchymal stem cell-derived exosomal miR-144–5p improves rat ovarian function after chemotherapy-induced ovarian failure by targeting PTEN. *Laboratory Investigation*, **100**(3): 342−352.

Yang ZL, Du X, Wang CL, et al. 2019. Therapeutic effects of human umbilical cord mesenchymal stem cell-derived microvesicles on premature ovarian insufficiency in mice. *Stem Cell Research & Therapy*, **10**(1): 250.

Younes MN, Yigitbasi OG, Yazici YD, et al. 2007. Effects of the integrin-linked kinase inhibitor QLT0267 on squamous cell carcinoma of the head and neck. *Archives of Otolaryngology-Head & Neck Surgery*, **133**(1): 15−23.

Zhang JY, Guan JJ, Niu X, et al. 2015. Exosomes released from human induced pluripotent stem cells-derived MSCs facilitate cutaneous wound healing by promoting collagen synthesis and angiogenesis. *Journal of Translational Medicine*, **13**: 49.

Zhang QW, Bu SX, Sun JY, et al. 2017. Paracrine effects of human amniotic epithelial cells protect against chemotherapy-induced ovarian damage. *Stem Cell Research & Therapy*, **8**(1): 270.

Zhang QW, Sun JY, Huang YT, et al. 2019. Human amniotic epithelial cell-derived exosomes restore ovarian function by transferring MicroRNAs against apoptosis. *Molecular Therapy Nucleic Acids*, **16**: 407−418.

Zhang WH, Ji H, Wang JL, et al. 2014. Garnulosa cells model tansfected by ENO1 overexpression adenovirus vector and the effect of ENO1 overexpression on progesterone secretion. *Chinese Journal of Applied Physiology*, **30**(1): 85−88. (in Chinese)